STRUCTURAL CHEMISTRY

ISSN 2053-2296

Structural investigations of benzoyl fluoride and the benzoacyl cation of low-melting compounds and reactive intermediates

Valentin Bockmair,* Martin Regnat, Huu Khanh Trinh Tran and Andreas J. Kornath‡

Department Chemie, Ludwig-Maximilians Universität, Butenandtstrasse 5-13 (Haus D), D-81377 München, Germany.
*Correspondence e-mail: valentin.bockmair@cup.uni-muenchen.de

Received 25 September 2024
Accepted 18 January 2025

Edited by A. G. Oliver, University of Notre Dame, USA

‡ Deceased

Keywords: crystal structure; benzoacylium; benzoyl fluoride; acyl cation; acyl fluoride.

CCDC references: 2417958; 2417957

Supporting information: this article has supporting information at journals.iucr.org/c

Acyl fluorides and acyl cations represent typical reactive intermediates in organic reactions, such as Friedel–Crafts acylation. However, the comparatively stable phenyl-substituted compounds have not been fully characterized yet, offering a promising backbone. Attempts to isolate the benzoacylium cation have only been carried out starting from the acyl chloride with weaker chloride-based Lewis acids. Therefore, only adducts of 1,4-stabilized acyl cations could be obtained. Due to the low melting point of benzoyl fluoride, together with its volatility and sensitivity toward hydrolysis, the structures of the acyl fluoride and its acylium cation have not been determined. Herein, we report the first crystal structure of benzoyl fluoride, C_7H_5FO or PhCOF (monoclinic $P2_1/n$, $Z = 8$) and the benzoacylium undecafluorodiarsenate, $C_7H_5O^+ \cdot As_2F_{11}^-$ or $[PhCO]^+[As_2F_{11}]^-$ (monoclinic $P2_1/n$, $Z = 4$). The compounds were characterized by low-temperature vibrational spectroscopy and single-crystal X-ray analysis, and are discussed together with quantum chemical calculations. In addition, their specific π-interactions were elucidated.

1. Introduction

Benzoyl fluoride, the acyl fluoride of benzoic acid, was first described in the mid-19th century (Borodine, 1863). Although vibrational spectroscopy (Seewann-Albert & Kahovec, 1948; Green & Harrison, 1977; Kniseley *et al.*, 1962; Kakar, 1972) and theroetical calculations concerning the internal rotational barrier (Yadav *et al.*, 1987) were reported in the literature decades ago, the compound has not been structurally characterized, presumably due to its low melting point of 244.5 K (Jander & Schwiegk, 1961) and high sensitivity towards hydrolysis. The appropriate material properties of benzoyl fluoride make it essential as a construction material and depolymerization agent for silicones.

In contrast to the related acyl halides, benzoyl fluoride posesses low electrical conductivity, estimated to be due to self-dissociation (Scheme 1) as reported by Jander & Schwiegk (1961), which makes the compound a potent ionic liquid. The source of the conductivity was assumed to be the formation of the benzoacylium cation. The addition of a strong Lewis acid (L) to benzoyl fluoride resulted in a signifcant increase of the conductivity, which was referred to as the benzoyl cation, as well as LF after fluoride abstraction.

The trapping of these reactive aromatic intermediates of Friedel–Crafts acylation was further investigated in modern research to isolate the benzoyl chloride antimony pentachloride adduct, as well as the toluenacylium cation (Davlieva *et al.*, 2005). Nevertheless, despite much effort, the crystal

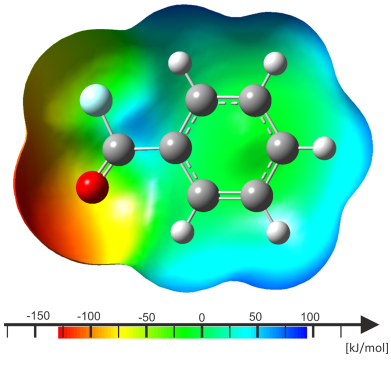

structure of benzoyl fluoride and the respective acylium ion could not be determined. Similar attempts were made to characterize the 1,4-diacylium cation of benzene (Olah & Comisarow, 1966). This raises the question whether a stabilizing effect of the *para* substitutent is needed for the abstraction of the halogen ion or only for acyl chlorides, as reported previously (Davlieva *et al.*, 2005).

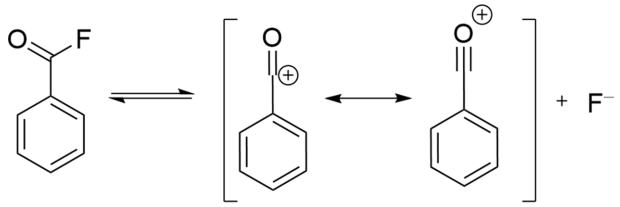

Scheme 1

Although there are many ways to synthesize benzoyl fluoride, a catalyst-free path was chosen. The synthesis path from benzoic acid with sulfur tetrafluoride was preferred, yielding benzoyl fluoride in high purity, only containing volatile by-products (Scheme 2). Arsenic pentafluoride was used for fluoride trapping due to its high fluoride ion affinity.

Besides the benzoic acid derivatives, investigations of the fluorinate and acylate terephthalic acid and isophthalic acid were performed to compare the stability and influence of the respective moieties on the aromatic system.

2. Experimental

Caution! Note that any contact with the described compounds should be avoided. Hydrolysis of AsF_5, SF_4, SOF_2 and the synthesized salts forms HF which burns the skin and causes irreparable damage. Safety precautions should be taken while handling these compounds.

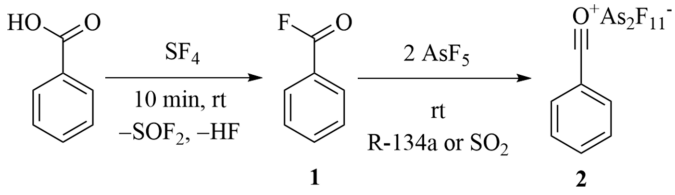

Scheme 2

All reactions were carried out by employing standard Schlenk techniques on a stainless steel vacuum line. The syntheses of the salts were performed using FEP (fluorinated ethylene–propylene copolymer)/PFA (perfluoroalkoxyalkane) reactors with stainless steel valves.

2.1. Synthesis and crystallization

Benzoic acid (65 mg, 0.532 mmol, 1 equiv.) was added to an FEP reactor in a nitrogen countercurrent flow. Sulfur tetrafluoride (116 mg, 1.07 mmol, 2 equiv.) was then condensed in a static vacuum in the reactor and frozen with liquid nitrogen. The reaction mixture was warmed to room temperature and homogenized until liquified. The generated thionyl fluoride and hydrogen fluoride were removed in a dynamic vacuum at 195 K. Benzoyl fluoride (**1**) was obtained as a colourless solid in quantitative yield.

For the crystallization of benzoyl fluoride (**1**), the crude product was recrystallized at 195 K under a cooled nitrogen stream to remove the last traces of thionyl fluoride and to solidify the saturated solution.

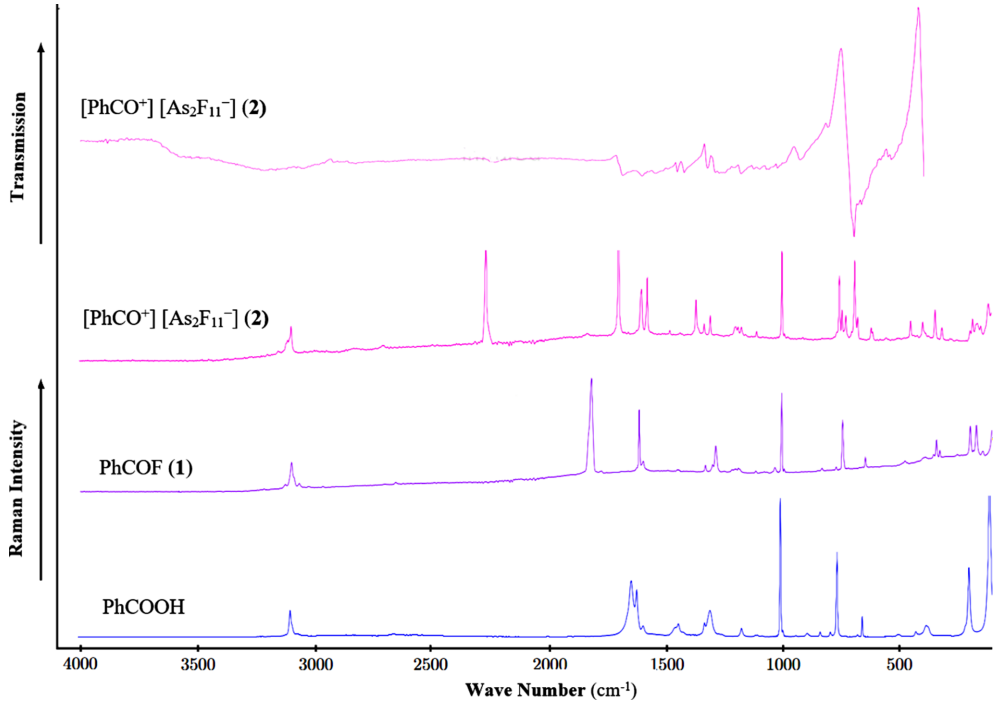

Figure 1
IR and Raman spectra of PhCOOH, PhCOF (**1**) and benzoacylium undecafluorodiarsenate (**2**).

Table 1
Experimental details.

For both structures: monoclinic, $P2_1/n$. Experiments were carried out with Mo $K\alpha$ radiation using a Rigaku Xcalibur Sapphire3 diffractometer. Absorption was corrected for by multi-scan methods (*CrysAlis PRO*; Rigaku OD, 2020).

	1	**2**
Crystal data		
Chemical formula	C_7H_5FO	$C_7H_5O^+\cdot As_2F_{11}^-$
M_r	124.11	463.95
Temperature (K)	114	112
a, b, c (Å)	12.592 (3), 7.2274 (17), 13.473 (3)	10.6376 (9), 9.9099 (7), 13.0019 (9)
β (°)	104.77 (2)	101.806 (8)
V (Å^3)	1185.6 (5)	1341.63 (18)
Z	8	4
μ (mm^{-1})	0.11	5.11
Crystal size (mm)	0.50 × 0.49 × 0.11	0.40 × 0.32 × 0.25
Data collection		
T_{min}, T_{max}	0.151, 1.000	0.213, 1.000
No. of measured, independent and observed [$I > 2\sigma(I)$] reflections	7905, 2413, 1506	13692, 3328, 2658
R_{int}	0.064	0.053
(sin $\theta/\lambda)_{max}$ (Å^{-1})	0.625	0.667
Refinement		
$R[F^2 > 2\sigma(F^2)]$, $wR(F^2)$, S	0.080, 0.249, 1.04	0.036, 0.095, 1.06
No. of reflections	2413	3328
No. of parameters	203	206
H-atom treatment	All H-atom parameters refined	H atoms treated by a mixture of independent and constrained refinement
$\Delta\rho_{max}$, $\Delta\rho_{min}$ (e Å^{-3})	0.38, −0.42	0.82, −0.61

Computer programs: *CrysAlis PRO* (Rigaku OD, 2020), *SHELXT* (Sheldrick, 2015*a*), *SHELXL2018* (Sheldrick, 2015*b*), *ORTEP-3 for Windows* (Farrugia, 2012) and *PLATON* (Spek, 2020).

Arsenic pentafluoride (904 mg, 5.32 mmol, 10 equiv.) was condensed in a static vacuum in the FEP reactor containing synthesized benzoyl fluoride (**1**) and then frozen with liquid nitrogen. Sulfur dioxide (2 ml) was condensed in the reactor and frozen in a static vacuum. The reaction mixture was warmed to room temperature and homogenized until the solution was clear. After the removal of excess arsenic pentafluoride and solvent, benzoacylium undecafluorodiarsenate (**2**) was obtained as a colourless solid in quantitative yield.

3. Analysis

The products PhCOF (**1**) and [PhCO][As_2F_{11}] (**2**) were characterized by single-crystal X-ray diffraction and low-temperature vibrational spectroscopy. In addition, quantum chemical calculations were perfomed with *GAUSSIAN* (Frisch *et al.*, 2016) to compare the observed frequencies and bond lengths, as well as displaying the mapped electrostatic potential using *GaussView* (Dennington *et al.*, 2016).

Single crystals of **1** and **2** suitable for single-crystal diffraction analysis were selected under a stereo microscope in a cooled nitrogen stream. Single crystals were prepared on a stainless steel polyamide micromount and the data collections were performed at 112 and 114 K, respectively, on an Xcalibur diffractometer system (Rigaku Oxford Diffraction). Details of the data collection and treatment, as well as structure solution and refinement, are available in the CIF in the supporting information.

Low-temperature vibrational spectroscopy measurements were performed to screen the conversion. IR spectroscopic investigations were carried out with a Bruker Vertex-80V FT–IR spectrometer using a cooled cell with a single-crystal CsBr plate on which small amounts of the samples were placed (Bayersdorfer *et al.*, 1972). For Raman measurements, a Bruker MultiRam FT–Raman spectrometer with Nd:YAG laser excitation (λ = 1064 nm) was used. The measurement was performed after transferring the sample to a cooled (77 K) glass cell under a nitrogen atmosphere and subsequent evacuation of the glass cell. The low-temperature IR spectra are depicted in Fig. 1.

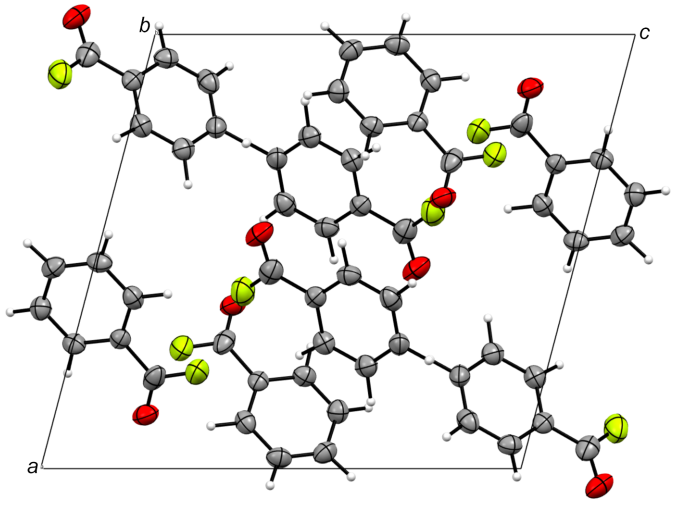

Figure 2
Crystal structure of benzoyl fluoride (**1**), viewed along the b axis. Displacement ellipsoids are drawn at the 50% probability level.

Table 2
Interatomic distances (Å) for benzoic acid, benzoyl chloride and the two independent rings in benzoyl fluoride.

'Lit' is literature, 'Exp' is experimental and 'Calc' is calculated (B3LYP/aug-cc-pVTZ).

$PhCO_2H$	Lit	PhCOCl	Lit	PhCOF 1	Exp	PhCOF 2	Exp	Calc
C═O	1.252	C═O	1.177 (3)	C1═O1	1.222 (4)	C14═O2	1.224 (4)	1.186
C—O	1.300	C—Cl	1.787 (2)	C7—F1	1.296 (5)	C14—F2	1.312 (4)	1.367
C1—C2	1.491	C7—C1	1.471 (3)	C7—C1	1.472 (4)	C7—C1	1.472 (3)	1.474
C2—C3	1.405	C1—C2	1.383 (3)	C1—C2	1.380 (5)	C1—C2	1.391 (4)	1.397
C3—C4	1.446	C2—C3	1.385 (3)	C2—C3	1.389 (4)	C2—C3	1.386 (3)	1.388
C4—C5	1.390	C3—C4	1.374 (4)	C3—C4	1.385 (4)	C3—C4	1.377 (4)	1.391
C5—C6	1.367	C4—C5	1.377 (4)	C4—C5	1.374 (5)	C4—C5	1.384 (5)	1.392
C6—C7	1.431	C5—C6	1.379 (3)	C5—C6	1.395 (4)	C5—C6	1.387 (4)	1.385
C2—C7	1.389	C6—C1	1.390 (3)	C6—C1	1.394 (3)	C6—C1	1.383 (4)	1.398

3.1. Crystal structure refinement

Basic crystallographic data and details of the data collection and structure refinement are summarized in Table 1 (Sheldrick, 2015*b*). For benzoyl fluoride (**1**), an alert for the Hirshfeld test was reported by *PLATON* (Spek, 2020). Therefore, a disordered O/F (*A*; 50:50 occupancy ratio) model was applied, improving the model compared with an ordered system in the course of structure refminement. The positions of the H atoms in the structure were localized in the difference Fourier map and refined without any restrictions. All atoms occupy the general position 4*e*.

For the refinement of the H-atom positions in the structure of [PhCO][As_2F_{11}] (**2**), the positions were localized from a difference Fourier map and refined without any restraints, with the exception of atom H3, which was idealized for an aromatic C—H distance and angles. All atoms occupy the general position 4*e*.

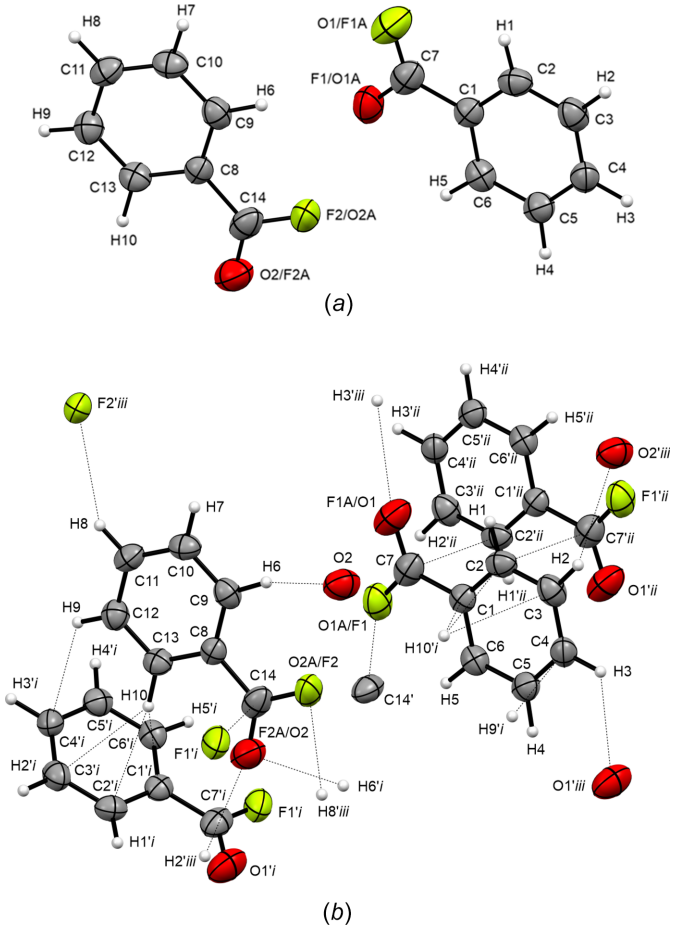

Figure 3
The asymmetric unit of (*a*) benzoyl fluoride (**1**) and (*b*) its short contacts with neighbouring molecules (′). Displacement ellipsoids are drawn at the 50% probability level. [Symmetry codes: (i) $-x+\frac{1}{2}, y+\frac{1}{2}, -z+\frac{1}{2}$; (ii) $-x, -y, -z$; (iii) $x+\frac{1}{2}, -y+\frac{1}{2}, z+\frac{1}{2}$.]

3.2. Crystal structure

Benzoyl fluoride (**1**) crystallizes in the monoclinic space group $P2_1/n$, with eight formula units per unit cell (Fig. 2). The asymmetric unit of **1** [Fig. 3(*a*)] is built up of two crystallographically independent molecules, with different chemical enviroments [Fig. 3(*b*)]. The two rings are formed by atoms C1–C6 and C8–C13. Benzoyl fluoride shows similar C—C bond lengths to benzoic acid and benzoyl chloride, considering the aromatic ring, as reported in Table 2. When the electron-withdrawing effect of the substituent is increased by converting the carboxylic acid group to acyl halogenide, the C_{Ph}—C bond is significantly shortened. The COF moiety has C═O bond lengths of 1.222 (4) and 1.224 (4) Å, whereas the C—F bond length is comparatively short with respect to already known acyl fluorides, with values of 1.296 (5) and 1.312 (4) Å (Durig *et al.*, 1998; van Eijck *et al.*, 1977; Bayer *et al.*, 2022*a*,*b*). This phenomenon can be rationalized by strong hyperconjugative effects of the arene ring on atom C7, but as the two rings in the asymmetric unit form different weak contacts, small deviations in the C—F bond lengths can be detected. The angles within the benzylic ring are within the 3σ rule [119.2 (3)–120.8 (3)°] and can therefore be regarded as idealized 120° angles in both parts of the asymmetric unit.

In the crystal structure, benzoyl fluoride is mainly stabilized either by C···*A* (*A* = O or F) interactions or aromatic interactions, as listed in Table 3. These contacts are 3.092 (4) (*A*1···C14), 3.295 (3) (*A*1···H3—C4), 3.398 (5) (*A*2···H2—C3), 3.461 (3) (*A*2···C11) and 3.520 (4) Å (O2···H6—C9). In addition, strong interactions of the π-systems were detected by parallel-displaced stacking at a distance of 3.328 Å (C2···$C7^{i}$) along the inversion centre at [0,0,0], and a T-shaped medium interaction (C13—H10···π; π–σ attraction) was detected at a distance of 3.476 Å (C13···*Cg*1; *Cg*1 is the

Table 3
Contacts (Å) of the benzoacyl cation in the structure of PhCOF (**1**).

Contact	Distance
F1···C14^{iii}	3.092 (4)
O1···(H3)^{ii}C4^{ii}	3.295 (3)
C2···C7^{i}	3.328 (5)
C3(H2)···O2^{ii}	3.398 (5)
C11(H8)···F2^{ii}	3.461 (3)
C9(H6)···O2^{iii}	3.520 (4)
C4···(H9^{iii})C12^{iii}	3.659 (5)
C3···(H10^{iii})C13^{iii}	3.775 (5)
C1···(H10^{iii})C13^{iii}	3.779 (4)
C2···(H10^{iii})C13^{iii}	3.823 (4)

Symmetry codes: (i) $-x+1, -y+1, -z+1$; (ii) $x-\frac{1}{2}, -y+\frac{1}{2}, z-\frac{1}{2}$; (iii) $-x+\frac{3}{2}, y-\frac{1}{2}, -z+\frac{1}{2}$.

Table 4
Interatomic distances (Å) for the benzoacyl cation and the CH_3CO^+ cation.

'Exp' is experimental, 'Calc' is calculated (B3LYP/aug-cc-pVTZ) and 'Lit' is literature.

PhCO$^+$	Exp	Calc	TolCO$^+$	Lit	CH_3CO^+	Lit
C≡O	1.109 (5)	1.126	C≡O	1.116 (2)	C≡O	1.116
C1—C7	1.403 (5)	1.378	C1—C7	1.391 (2)	C1—C2	1.378 (2)
C1—C2	1.404 (5)	1.417	C1—C2	1.405 (2)		
C2—C3	1.374 (5)	1.377	C2—C3	1.376 (2)		
C3—C4	1.380 (6)	1.397	C3—C4	1.402 (2)		
C4—C5	1.390 (5)	1.397	C4—C5	1.397 (2)		

centroid of the ring), as the C—H bond is tilted 30.14° with respect to the ring normal (Janiac, 2000).

Benzoacylium undecafluorodiarsenate (**2**) crystallizes in the monoclinic space group $P2_1/n$, with four formula units per unit cell (Fig. 4). The asymmetric unit [Fig. 5(*a*)] is built up of one $PhCO^+$ cation and one As_2F11^- anion. The C≡O bond length is in accordance with known bond lengths of acylium compounds, such as the CH_3CO^+ cation (Table 4; Boer, 1966), whereas the C—C bond is significantly elongated. Regarding the C_{Ph}—C bond length of 1.472 (4) Å in **2**, this bond is significantly shortened to 1.403 (5) Å in **1** by the stabilizing mesomeric effects of the π-system. The C—C bond lengths within the arene ring are similar to those of **1**. The angles in the arene ring are close to the idealized angle (120°) and are in the range 117.4 (4)–122.8 (3)°. The bond lengths of the undecafluorodiarsenate ($[As_2F_{11}]^-$) anion are consistent with values reported in the literature (Minkwitz & Neikes, 1999).

Table 5
Contacts (Å) of the benzoacyl cation in the structure of $[PhCO][As_2F_{11}]$.

Contact	Distance
C7···F3	2.803 (4)
C7···F11^{i}	2.873 (4)
O1···F8^{ii}	2.893 (3)
C7···F9^{iii}	2.900 (5)
C7···F4^{ii}	2.986 (4)
O1···F3	2.988 (4)
C6···F3	2.997 (5)
C7···F7^{i}	3.102 (4)
C1···F3	3.145 (4)
C4···F1^{ii}	3.151 (4)
C6(H5)···F7^{i}	3.284 (5)
C5(H4)···F5^{iii}	3.417 (5)
C4(H3)···F1^{iii}	3.451 (5)
O1···plane(ring)/O1···centroid(C1–C6)	3.394/3.428

Symmetry codes: (i) $-x, -y, -z$; (ii) $-x+\frac{1}{2}, y+\frac{1}{2}, -z+\frac{1}{2}$; (iii) $x+\frac{1}{2}, -y+\frac{1}{2}, z+\frac{1}{2}$.

Within its packing, the benzoacylium cation is surrounded by six $[As_2F_{11}]^-$ anions [Fig. 5(*b*)] and forms C···F contacts, as well as a T-shaped π-interaction (Table 5). The six C···F contacts formed by the acylium moiety are in the range 2.803 (4)–3.151 (4) Å. Except for one C···F contact (C6···F3) of 2.997 (5) Å, the interactions with the arene ring are weaker considering the F···H—C distances of 3.284 (5)–3.451 (5) Å. It is noticeable that the contacts of C2—H1 strongly differ from those of other aromatic contacts, because its contact to the anion has a distance of 3.769 (5) Å. The benzoacylium cation shows rare T-shaped π-stacking in the crystal structure [π–σ(CO) interactions]. The closest contacts of the benzoacylium cations with itself are 3.394 (ring-plane···O1) and

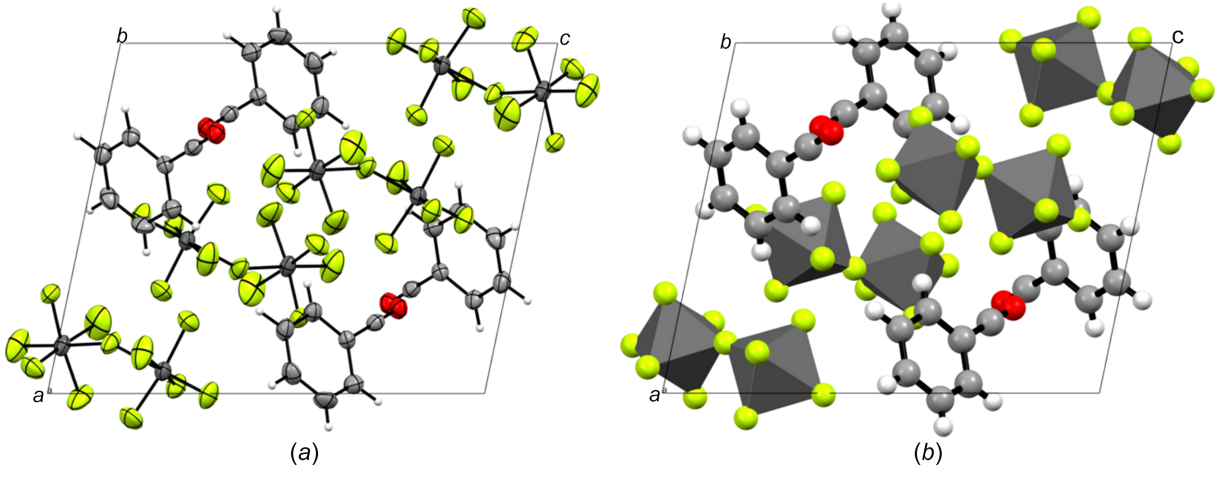

Figure 4
The crystal structure of benzoacylium undecafluorodiarsenate (**2**), viewed along the *b* axis, (*a*) with displacement ellipsoids and (*b*) in a polyhedral illustration. Displacement ellipsoids are drawn at the 50% probability level.

Table 6
Measured and calculated vibration frequencies (cm^{-1}) for $PhCO_2H$.

Raman	Calc[a,b] (Raman/IR)[c]	Assignment
	3627 (138/94)	ν(O—H)
3073 (42)	3104 (121/2)	ν(C—H)
3063 (28)	3098 (102/4)	ν(C—H)
3039 (5)	3084 (135/12)	ν(C—H)
3009 (6)	3075 (98/10)	ν(C—H)
2982 (4)	3063 (52/0)	ν(C—H)
	1721 (89/367)	ν(C═O)
1634 (18)	1588 (75/18)	ν(C═C)
1602 (32)	1569 (6/5)	ν(C═C)
	1478 (1/1)	δ(C═C)
1443 (4)	1437 (2/15)	δ(C═C)
1324 (7)	1320 (12/115)	δ(C—COH)
	1310 (1/4)	δ(C═C)
1290 (14)	1295 (1/2)	ν(C═C)
1180 (7)	1170 (12/60)	δ(C—H)
1170 (4)	1150 (22/160)	δ(C—H) + ν(C—C)
1158 (4)	1145 (6/1)	δ(C—H)
1133 (6)	1078 (1/41)	δ(C—H)
	1055 (0/119)	δ(C═C)
1028 (14)	1014 (11/19)	δ(C═C)
	992 (0/0)	δ(C—H)
1002 (100)	989 (45/0)	Ring breathing
991 (3)	978 (0/0)	τ(C—H)
	940 (0/1)	τ(C—H)
	845 (0/0)	τ(C—H)
812 (5)	801 (1/0)	δ(C—H)
	750 (18/8)	δ(C—C═C)
	708 (0/123)	τ(C—H)
	685 (0/8)	ω(C—C═C)
618 (14)	618 (1/48)	δ(C—C═C)
	612 (5/0)	δ(C—C═C)
	575 (2/61)	τ(O—H)
	480 (1/6)	δ(C—COH)
421 (10)	423 (0/9)	δ(C—C═C)
	401 (0/0)	ω(C—C═C)
	371 (4/5)	δ(C—C═C)
195 (21)	210 (0/2)	δ(C—CO_2H)
	153 (2/1)	δ(CO_2H)
	60 (0/1)	ω(CO_2H)

Notes: (*a*) calculated at the B3LYP/aug-cc-pVTZ level; (*b*) scaling factor 0.967; (*c*) IR intensities in kJ mol^{-1} and Raman intensities in $Å^4$/AMU or % at observed frequencies.

3.428 Å (centroid···O1), and can be regarded as medium strong (Janiac, 2000). The acylium moiety is nearly perpendicular to the centre of neighbouring ring systems [Fig. 5(*b*)], with deviating angles ranging from 81.82 (O1···centroid···C5) to 97.86° (O1···centroid···C3).

3.3. Quantum chemical calculations

The quantum chemical calculations were performed at the aug-cc-pVTZ-level of theory at 298 K with the *GAUSSIAN16* program package (Frisch *et al.*, 2016).

The structures were opimized using DFT methods for the calculation of vibration frequencies. For futher energetic calculations, such as the mapped electrotatic potential, MP2 methods were applied for more accurate energy values.

As depicted in Table 2, the deviations between the calculated and observed bond lengths are in good agreement. Since the interactions within the crystal structure appear to be only weak, no further modelling of contacts was necessary for the calculations. The electron-withdrawing shift towards the substituent can be seen in the mapped electostatic potential (Fig. 6). The electron-poor carbonyl C atom inhibits an electron hole (blue), as it is attached to the highly electronegative F and O atoms.

The calculations for $PhCO^+$ are also in accordance with the observed bond lengths, as illustrated in Table 3, so that values are close to the 3σ rule. The comparable slightly higher deviation can be rationalized by the influence of stronger interactions. As visualized by the mapped electrostatic potential (Fig. 7), a π-hole (blue) is localized at atom C7.

Comparing the calculations, a similar mapped electrostatic potential has already been calculated for fumaryl fluoride monoacylium, which posesses both functional groups, *i.e.* acylium and an acyl fluoride moiety (Bayer *et al.*, 2022*a*).

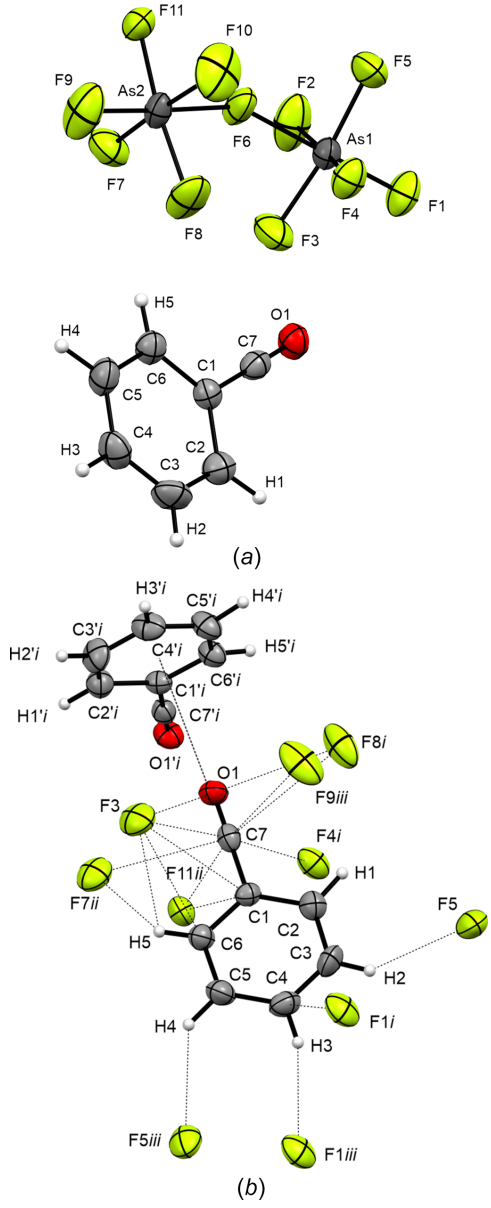

Figure 5
(*a*) The asymmetric unit of [PhCO][As_2F_{11}] (**2**) and (*b*) short contacts of the benzoacylium cation. Displacement ellipsoids are drawn at the 50% probability level. [Symmetry codes: (i) $-x+\frac{1}{2}, y+\frac{1}{2}, -z+\frac{1}{2}$; (ii) $-x, -y, -z$; (iii) $x+\frac{1}{2}, -y+\frac{1}{2}, z+\frac{1}{2}$.]

Table 7
Measured and calculated vibration frequencies (cm^{-1}) for PhCOF.

Raman	Calc[a,b] (Raman/IR)[c]	Assignment
	3107 (120/2)	ν(C—H)
	3098 (121/4)	ν(C—H)
3084 (21)	3086 (115/9)	ν(C—H)
3075 (27)	3078 (95/8)	ν(C—H)
3061 (9)	3066 (51/0)	ν(C—H)
1809 (48)		
1795 (31)	1797 (132/404)	ν(C═O)
1758 (36)		
1602 (100)	1587 (75/24)	ν(C═C)
1589 (11)	1569 (5/2)	ν(C═C)
1494 (3)	1477 (0/1)	ν(C═C)
1457 (3)	1437 (1/14)	ν(C═C)
1323 (3)	1312 (1/4)	δ(C—H)
1268 (13)	1296 (0/2)	ν(C═C)
1246 (13)	1216 (33/217)	ν(C—COF)
1178 (8)	1161 (5/27)	δ(C—H)
1167 (18)	1147 (5/1)	δ(C—H)
	1073 (1/2)	δ(C═C)
1018 (10)	1019 (6/16)	δ(C═C)
1011 (7)	995 (0/0)	ν(C—F)
	990 (23/165)	δ(C═C)
1002 (98)	988 (28/22)	Ring breathing
	978 (0/0)	δ(C—H)
	941 (0/1)	δ(C—H)
855 (2)	844 (0/0)	δ(C—H)
787 (9)	793 (1/3)	δ(C—H)
771 (28)	749 (17/15)	δ(C—C═C)
	696 (0/96)	δ(C—H)
	678 (0/1)	δ(C—C═C)
	632 (0/17)	δ(C—C═C)
617 (21)	611 (5/1)	δ(C—COF)
492 (3)	477 (2/1)	δ(C—C═C)
	427 (0/0)	ω(C—C═C)
	401 (0/0)	τ(C—C)
382 (15)	366 (4/3)	δ(C—C═C)
217 (4)	205 (0/1)	δ(C—COF)
187 (24)		
173 (21)	153 (2/0)	δ(C═O)
	64 (1/0)	τ(COF)

Notes: (*a*) calculated at the B3LYP/aug-cc-pVTZ level; (*b*) scaling factor 0.967; (*c*) IR intensities in kJ mol^{-1} and Raman intensities in $Å^4$/AMU or % at observed frequencies.

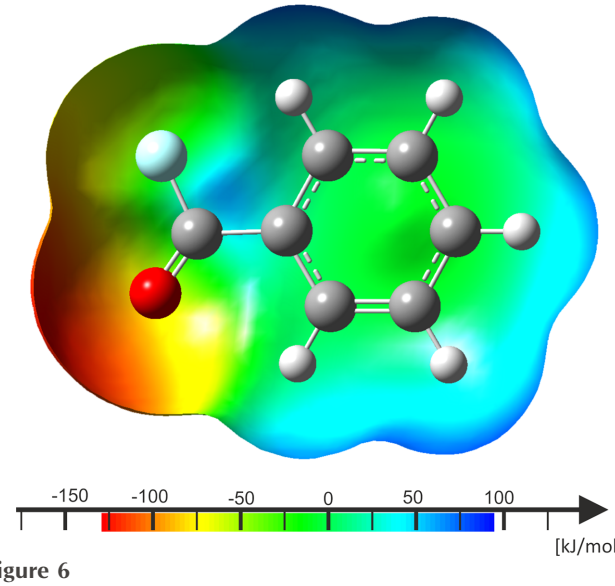

Figure 6
Calculated mapped electrostatic potential onto an electron-density isosurface value of 0.0004 $Bohr^{-3}$, with the colour scale ranging from −127.074 (red) to 87.692 kJ mol^{-1} (blue) of PhCOF.

Table 8
Measured vibrations for [PhCO][As_2F_{11}] and calculated vibration frequencies (cm^{-1}) for $[PhCO]^+$.

Raman	Calc[a,b]	(Raman/IR)[c]	Assignment
3167 (5)	3167 (*s*)	3109 (302/1)	ν(C—H)
3144 (5)		3107 (6/12)	ν(C—H)
3137 (5)		3098 (37/6)	ν(C—H)
3108 (14)	3107 (*s*)	3096 (91/0)	ν(C—H)
3088 (23)	3084 (*s*)	3087 (42/0)	ν(C—H)
2253 (8)			
2232 (46)	2233 (*s*)	2211 (144/930)	ν(C≡O)
2223 (63)			
1583 (100)	1601 (*s*)	1564 (51/152)	ν(C═C)
		1536 (1/0)	ν(C═C)
1451 (5)	1450 (*s*)	1455 (2/2)	ν(C═C)
		1428 (1/43)	ν(C═C)
1328 (4)	1321 (*s*)	1330 (1/16)	ν(C═C)
		1292 (0/1)	ν(C═C)
1182 (13)	1192 (*s*)	1207 (2/54)	ν(C—CO)
1177 (10)	1178 (*s*)	1166 (4/3)	δ(C═C)
1158 (15)		1164 (3/65)	ν(C—CO)
1104 (4)		1085 (1/1)	ν(C═C)
1021 (16)	1030 (*s*)	1020 (0/0)	ν(C═C)
		1002 (16/0)	δ(C═C)
		984 (0/0)	τ(C—H)
997 (74)	999 (*s*)	974 (36/11)	Ring breathing
		951 (0/1)	τ(C—H)
		823 (0/0)	τ(C—H)
763 (15)			
751 (13)		755 (0/42)	δ(C—H)
740 (17)		748 (21/1)	δ(C—CO)
725 (7)	696 (*vs*)	646 (0/32)	
639 (12)		636 (2/4)	δ(C—CO)
609 (10)		584 (3/3)	δ(C—CO)
		583 (0/27)	δ(CO)
452 (43)		442 (15/4)	δ(C—C═C)
		378 (0/0)	ω(C—C═C)
370 (8)		370 (0/0)	δ(C—H)
311 (12)			
172 (12)			
160 (16)			
152 (13)		147 (1/2)	δ(C≡O)
		125 (1/0)	δ(C—CO)
As_2F_{11}			
740 (17)			ν(As—F)
685 (60)	685 (*s*)		ν(As—F)
586 (9)			δ(As—F)
393 (11)			δ(As—F)

Notes: (*a*) calculated at the B3LYP/aug-cc-pVTZ level; (*b*) scaling factor 0.967; (*c*) IR intensities in kJ mol^{-1} and Raman intensities in $Å^4$/AMU or % at observed frequencies.

3.4. Vibrational spectroscopy

Experimental vibrational frequencies for benzoyl fluoride and the benzoacylium cation were assigned according to Tables 6, 7 and 8, in accordance with quantum chemical calculations at the B3LYP/aug-cc-pVTZ level of theory, and compared to the starting material, benzoic acid (Fig. 1).

C_1 symmetry was determined for benzoyl fluoride and the benzoacylium cation, with 36 and 33 fundamental vibrational modes (A), respectively. All observed vibrational frequencies were assigned with the aid of quantum chemical calculations, as listed in Tables 5 and 6.

The successful synthesis of the acylium ion is indicated by the stretching vibration of the carbonyl group. The ν(C═O) is assigned to the Raman line at 1634 cm^{-1} in the vibrational spectrum of the starting material and is no longer observed in

the vibrational spectrum of **2**. The C≡O stretching vibration of the acyl cation is detected in the Raman spectrum at 2232 cm^{-1} for **2** and in the IR spectrum at 2233 cm^{-1} for **2**. The successful fluoride abstraction was also observed by the absence of the C—F stretching vibration and the COF bending vibrations of the neutral compound in the vibrational spectra of **2**. These are detected in the Raman spectrum of the starting material at 1246 and 617 cm^{-1}, respectively, but are no longer observed in the vibrational spectra of **2**. The antisymmetric C—C—OH bending vibration present in the Raman spectrum of benzoic acid at 1324 cm^{-1} was also not detected in the Raman spectra of fluoride **1** and acylium salt **2**. The Raman lines of the C_{Ph}—C vibrations were detected blue-shifted from 1150 (benzoic acid) to 1216 (**1**) and 1207 cm^{-1} (**2**). The benzene ring breathing modes are detected in the Raman spectra of **1** and **2** at 1002 and 997 cm^{-1}, respectively, and remain unchanged after the transformation of benzoic acid to benzoyl fluoride and fluoride abstraction (5 cm^{-1} blue-shifted). The same trend was observed for ν(C=C), which are not affected by the conversion of benzoic acid to **1** (1602 cm^{-1}) and **2** (1583 cm^{-1}). The C—H stretching vibrations of the arene ring are observed at 3084, 3075 and 3061 cm^{-1} in **1**, and at 3167, 3108 and 3088 cm^{-1} in **2**, and are red-shifted in comparison with benzoic acid.

The vibrational frequencies of the $[As_2F_{11}]^-$ anions are in accordance with values reported in the literature (Minkwitz & Neikes, 1999) and are listed in Table 6.

4. Conclusion

Herein we report the first crystal structures of the smallest benzylic acyl fluoride and the acyl cation, as well as their vibrational characterization. The strong carbon bond towards the C—COF or C—CO^+ moiety, respectively, can be rationalized by the strong strengthening effects of π–π hyperconjugation of the arene subsituent analog to the toluene acylium ion. The strengthening effect is also visable in the blue shift of the Raman lines and is therefore consistent with the calculated values and obtained crystallographic data. Although the compounds are stable up to room temperature, the acyl fluoride shows a high volatility even at low temperatures.

The challenging crystallization of low-melting volatile compounds such as acyl fluorides can succeed starting from saturated solutions with volatile solvents under a cool nitrogen stream by recrystallization, such as was observed for benzoyl fluoride.

Analogous to the reported benzoic acid derivatives, terephthalic acid and isophthalic acid were reacted, but the products could not be crystallized due to a change of solubility. A change of the solvent thionyl fluoride to 1,1,1,2-tetrafluoroethane (R-134a) or mixtures might lead to successful isolation.

A stabilizing *para*-substituent effect appears not to be necessary when performing the abstraction with antimony pentafluoride. In contrast to the experiments of Davlieva *et al.* (2005), the acyl cation was obtained instead of the $SbCl_5$ adduct. Therefore, it can be deduced that the abstraction of halogenide with antimony chloride containing Lewis acids only succeeds for stabilized aromatics, whereas the abstraction with antimony pentafluoride can access acyl cations of less stabilized aromatics.

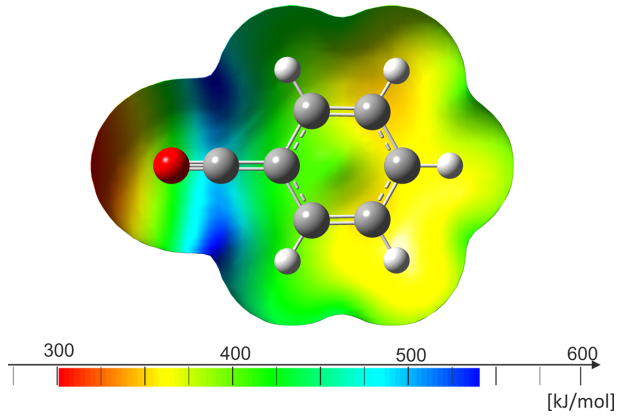

Figure 7
Calculated mapped electrostatic potential onto an electron-density isosurface value of 0.0004 $Bohr^{-3}$, with the colour scale ranging from 301.933 (red) to 538.228 kJ mol^{-1} (blue) of [PhCO][As_2F_{11}].

Acknowledgements

We are grateful to the Ludwig-Maximilian University of Munich, the Deutsche Forschungsgemeinschaft (DFG) and the F-Select GmbH for their support, as well as Professor Karaghiosoff for supervising this work. In particular, VB would like to thank Dr Constantin Hoch and Dr Sebastian Steiner for fruitful discussions. Open access funding enabled and organized by Projekt DEAL.

References

Bayer, M. C., Greither, N., Jessen, C., Nitzer, A. & Kornath, A. J. (2022*a*). *Eur. J. Inorg. Chem.* **2022**, e202200391.
Bayer, M. C., Kremser, C., Jessen, C., Nitzer, A. & Kornath, A. J. (2022*a*). *Chem. A Eur. J.* **28**, e202104422.
Bayersdorfer, L., Minkwitz, R. & Jander, J. (1972). *Z. Anorg. Allg. Chem.* **392**, 137–142.
Boer, P. (1966). *J. Am. Chem. Soc.* **88**, 1572–1574.
Borodine, A. (1863). *Justus Liebigs Ann. Chem.* **126**, 58–62.
Davlieva, M. G., Lindeman, S. V., Neretin, I. S. & Kochi, J. K. (2005). *J. Org. Chem.* **70**, 4013–4021.
Dennington, R., Keith, T. A. & Millam, J. M. (2016). *GaussView*. Version 6.0. Semichem Inc., Shawnee, Mission, KS, USA.
Durig, J. R., Guirgis, G. A. & Mohamed, T. A. (1998). *J. Mol. Struct.* **444**, 165–182.
Eijck, B. P. van (1977). *J. Mol. Struct.* **37**, 1–15.
Farrugia, L. J. (2012). *J. Appl. Cryst.* **45**, 849–854.
Frisch, M. J., Trucks, G. W., Schlegel, H. B., Scuseria, G. E., Robb, M. A., Cheeseman, J. R., Scalmani, G., Barone, V., Mennucci, B., Petersson, G. A., Nakatsuji, H., Caricato, M., Li, X., Hratchian, H. P., Izmaylov, A. F., Bloino, J., Zheng, G., Sonnenberg, J. L., Hada, M., Ehara, M., Toyota, K., Fukuda, R., Hasegawa, J., Ishida, M., Nakajima, T., Honda, Y., Kitao, O., Nakai, H., Vreven, T., Montgomery, J. A., Peralta, J. E., Ogliaro, F., Bearpark, M., Heyd, J. J., Brothers, E., Kudin, K. N., Staroverov, V. N., Kobayashi, R., Normand, J., Raghavachari, K., Rendell, A., Burant, J. C., Iyengar, S. S., Tomasi, J., Cossi, M., Rega, N., Millam, J. M., Klene, M., Know,

J. E., Cross, J. B., Bakken, V., Adamo, C., Jaramillo, J., Gomperts, R., Stratmann, R. E., Yazyev, O. A., Austin, J., Cammi, R., Pomelli, C., Ochterski, J. O., Martin, R. L., Morokuma, K., Zakrzweski, V. G., Voth, G. A., Salvador, P., Dannenberg, J. J., Dapprich, S., Daniels, A. D., Farkas, O., Foresman, J. B., Ortiz, J. V., Cioslowski, J. & Fox, D. J. (2016). *GAUSSIAN16*. Revision C.01. Gaussian Inc., Wallingford, CT, USA. https://gaussian.com/.

Green, J. H. S. & Harrison, D. J. (1977). *Spectrochim. Acta A*, **33**, 193–197.

Jander, G. & Schwiegk, L. (1961). *Z. Anorg. Allg. Chem.* **310**, 1–11.

Janiac, C. (2000). *J. Chem. Soc. Dalton Trans.* **2000**, 3885–3896.

Kakar, R. K. (1972). *J. Chem. Phys.* **56**, 1189–1197.

Kniseley, R. N., Fasse, V. A., Farquhar, E. L. & Gray, L. S. (1962). *Spectrochim. Acta*, **18**, 1217–1230.

Minkwitz, R. & Neikes, F. (1999). *Inorg. Chem.* **38**, 5960–5963.

Olah, G. A. & Comisarow, M. B. (1966). *J. Am. Chem. Soc.* **88**, 3313–3317.

Rigaku OD (2020). *CrysAlis PRO*. Rigaku Oxford Diffraction Ltd, Yarnton, Oxfordshire, England.

Seewann-Albert, H. & Kahovec, L. (1948). *Acta Phys. Aust.* **1**, 352.

Sheldrick, G. M. (2015*a*). *Acta Cryst.* A**71**, 3–8.

Sheldrick, G. M. (2015*b*). *Acta Cryst.* C**71**, 3–8.

Spek, A. L. (2020). *Acta Cryst.* E**76**, 1–11.

Yadav, R. A., Ram, S., Shanker, R. & Singh, I. S. (1987). *Spectrochim. Acta A*, **43**, 901–909.

supporting information

Acta Cryst. (2025). C**81**, 93-101 [https://doi.org/10.1107/S2053229625000476]

Structural investigations of benzoyl fluoride and the benzoacyl cation of low-melting compounds and reactive intermediates

Valentin Bockmair, Martin Regnat, Huu Khanh Trinh Tran and Andreas J. Kornath

Computing details

Benzoacylium undecafluorodiarsenate (xk047)

Crystal data

$C_7H_5O^+ \cdot As_2F_{11}^-$
M_r = 463.95
Monoclinic, $P2_1/n$
a = 10.6376 (9) Å
b = 9.9099 (7) Å
c = 13.0019 (9) Å
β = 101.806 (8)°
V = 1341.63 (18) Å^3
Z = 4
$F(000)$ = 880
D_x = 2.297 Mg m^{-3}
Mo $K\alpha$ radiation, λ = 0.71073 Å
Cell parameters from 3582 reflections
θ = 2.6–30.4°
μ = 5.11 mm^{-1}
T = 112 K
Block, colorless
0.40 × 0.32 × 0.25 mm

Data collection

Rigaku Xcalibur Sapphire3 diffractometer
Radiation source: Enhance (Mo) X-ray Source
Graphite monochromator
Detector resolution: 15.9809 pixels mm^{-1}
ω scans
Absorption correction: multi-scan (CrysAlis PRO; Rigaku OD, 2020)
T_{min} = 0.213, T_{max} = 1.000
13692 measured reflections
3328 independent reflections
2658 reflections with $I > 2\sigma(I)$
R_{int} = 0.053
θ_{max} = 28.3°, θ_{min} = 2.3°
h = −13→14
k = −13→13
l = −17→13

Refinement

Refinement on F^2
Least-squares matrix: full
$R[F^2 > 2\sigma(F^2)]$ = 0.036
$wR(F^2)$ = 0.095
S = 1.06
3328 reflections
206 parameters
0 restraints
Primary atom site location: structure-invariant direct methods
Secondary atom site location: difference Fourier map
Hydrogen site location: mixed
H atoms treated by a mixture of independent and constrained refinement
$w = 1/[\sigma^2(F_o^2) + (0.0448P)^2]$ where $P = (F_o^2 + 2F_c^2)/3$
$(\Delta/\sigma)_{max}$ = 0.001
$\Delta\rho_{max}$ = 0.82 e Å^{-3}
$\Delta\rho_{min}$ = −0.61 e Å^{-3}

Special details

Geometry. All esds (except the esd in the dihedral angle between two l.s. planes) are estimated using the full covariance matrix. The cell esds are taken into account individually in the estimation of esds in distances, angles and torsion angles; correlations between esds in cell parameters are only used when they are defined by crystal symmetry. An approximate (isotropic) treatment of cell esds is used for estimating esds involving l.s. planes.

Refinement. Refinement of F^2 against ALL reflections. The weighted R-factor wR and goodness of fit S are based on F^2, conventional R-factors R are based on F, with F set to zero for negative F^2. The threshold expression of $F^2 > 2\text{sigma}(F^2)$ is used only for calculating R-factors(gt) etc. and is not relevant to the choice of reflections for refinement. R-factors based on F^2 are statistically about twice as large as those based on F, and R- factors based on ALL data will be even larger.

Fractional atomic coordinates and isotropic or equivalent isotropic displacement parameters (Å²)

	x	*y*	*z*	U_{iso}*/U_{eq}
As1	0.43636 (3)	0.40022 (4)	0.75390 (3)	0.03148 (12)
As2	0.36296 (3)	0.19944 (4)	0.51094 (3)	0.03275 (12)
F11	0.21546 (19)	0.2613 (2)	0.45947 (16)	0.0435 (5)
F4	0.4790 (2)	0.2398 (2)	0.79122 (17)	0.0461 (6)
F6	0.3560 (2)	0.3246 (2)	0.62120 (16)	0.0521 (6)
F1	0.5051 (2)	0.4683 (2)	0.86996 (18)	0.0528 (6)
F7	0.4262 (2)	0.3296 (2)	0.4541 (2)	0.0552 (6)
F5	0.2937 (2)	0.3740 (3)	0.7883 (2)	0.0592 (7)
F3	0.5706 (2)	0.4121 (3)	0.7036 (2)	0.0597 (7)
O1	0.7572 (2)	0.6384 (3)	0.76211 (19)	0.0382 (6)
F2	0.3836 (3)	0.5484 (3)	0.6978 (2)	0.0692 (8)
F8	0.5112 (2)	0.1569 (3)	0.5770 (2)	0.0670 (8)
F9	0.3640 (3)	0.0947 (3)	0.4093 (2)	0.0729 (9)
F10	0.2981 (3)	0.0887 (3)	0.5819 (2)	0.0818 (10)
C7	0.7976 (3)	0.5606 (4)	0.7168 (3)	0.0317 (7)
C1	0.8470 (3)	0.4608 (3)	0.6596 (3)	0.0283 (7)
C6	0.7678 (4)	0.4094 (4)	0.5687 (3)	0.0342 (8)
C2	0.9736 (4)	0.4164 (4)	0.6962 (3)	0.0385 (8)
C5	0.8173 (4)	0.3110 (4)	0.5132 (3)	0.0420 (9)
C4	0.9426 (4)	0.2667 (4)	0.5489 (3)	0.0427 (9)
H3	0.976511	0.199599	0.510020	0.051*
C3	1.0191 (4)	0.3176 (4)	0.6393 (4)	0.0452 (10)
H1	1.023 (3)	0.460 (4)	0.760 (3)	0.036 (10)*
H4	0.765 (4)	0.280 (4)	0.446 (3)	0.049 (12)*
H5	0.687 (3)	0.442 (3)	0.542 (3)	0.026 (9)*
H2	1.096 (4)	0.281 (4)	0.659 (3)	0.052 (13)*

Atomic displacement parameters (Å²)

	U^{11}	U^{22}	U^{33}	U^{12}	U^{13}	U^{23}
As1	0.0354 (2)	0.0332 (2)	0.02547 (19)	0.00097 (13)	0.00528 (15)	−0.00178 (14)
As2	0.0424 (2)	0.0292 (2)	0.02471 (19)	0.00690 (14)	0.00230 (15)	0.00008 (14)
F11	0.0383 (11)	0.0549 (14)	0.0337 (12)	0.0035 (10)	−0.0008 (10)	−0.0016 (10)
F4	0.0566 (13)	0.0383 (12)	0.0394 (12)	0.0066 (10)	0.0004 (11)	0.0026 (10)
F6	0.0469 (13)	0.0710 (16)	0.0328 (12)	0.0194 (11)	−0.0049 (10)	−0.0198 (11)

F1	0.0691 (16)	0.0482 (14)	0.0360 (12)	−0.0048 (11)	−0.0014 (11)	−0.0128 (10)
F7	0.0509 (14)	0.0601 (16)	0.0612 (16)	−0.0014 (11)	0.0271 (12)	0.0115 (13)
F5	0.0422 (13)	0.088 (2)	0.0517 (15)	0.0022 (12)	0.0188 (12)	−0.0139 (14)
F3	0.0481 (14)	0.0775 (19)	0.0601 (16)	−0.0154 (12)	0.0267 (12)	−0.0035 (14)
O1	0.0434 (14)	0.0383 (15)	0.0331 (13)	0.0054 (11)	0.0083 (11)	−0.0066 (11)
F2	0.109 (2)	0.0489 (15)	0.0449 (14)	0.0241 (14)	0.0049 (15)	0.0064 (12)
F8	0.0629 (16)	0.0732 (18)	0.0551 (15)	0.0410 (13)	−0.0105 (13)	−0.0132 (14)
F9	0.106 (2)	0.0535 (16)	0.0506 (15)	0.0245 (14)	−0.0050 (15)	−0.0241 (13)
F10	0.114 (3)	0.0580 (18)	0.0721 (19)	−0.0231 (16)	0.0173 (18)	0.0312 (15)
C7	0.0300 (16)	0.0331 (18)	0.0299 (17)	−0.0018 (13)	0.0009 (14)	0.0045 (15)
C1	0.0327 (16)	0.0255 (17)	0.0279 (16)	0.0030 (12)	0.0091 (14)	0.0016 (13)
C6	0.0378 (18)	0.0332 (19)	0.0309 (18)	0.0064 (14)	0.0055 (16)	0.0005 (15)
C2	0.0351 (18)	0.041 (2)	0.039 (2)	−0.0003 (15)	0.0058 (17)	−0.0008 (17)
C5	0.049 (2)	0.046 (2)	0.0292 (19)	0.0067 (17)	0.0051 (17)	−0.0041 (16)
C4	0.049 (2)	0.042 (2)	0.041 (2)	0.0138 (17)	0.0180 (19)	−0.0005 (17)
C3	0.0300 (18)	0.050 (2)	0.056 (2)	0.0138 (16)	0.0094 (18)	0.000 (2)

Geometric parameters (Å, º)

As1—F1	1.678 (2)	As2—F7	1.693 (2)
As1—F2	1.684 (2)	As2—F6	1.909 (2)
As1—F5	1.688 (2)	O1—C7	1.109 (4)
As1—F3	1.692 (2)	C7—C1	1.403 (5)
As1—F4	1.697 (2)	C1—C6	1.399 (5)
As1—F6	1.9147 (19)	C1—C2	1.404 (5)
As2—F10	1.671 (3)	C6—C5	1.380 (5)
As2—F9	1.682 (2)	C2—C3	1.374 (5)
As2—F8	1.688 (2)	C5—C4	1.390 (5)
As2—F11	1.690 (2)	C4—C3	1.380 (6)
F1—As1—F2	94.86 (12)	F8—As2—F11	170.89 (11)
F1—As1—F5	94.24 (12)	F10—As2—F7	170.83 (14)
F2—As1—F5	90.62 (14)	F9—As2—F7	93.44 (14)
F1—As1—F3	94.15 (13)	F8—As2—F7	89.94 (14)
F2—As1—F3	90.25 (14)	F11—As2—F7	88.30 (11)
F5—As1—F3	171.47 (12)	F10—As2—F6	85.86 (14)
F1—As1—F4	94.44 (11)	F9—As2—F6	176.91 (11)
F2—As1—F4	170.69 (12)	F8—As2—F6	87.49 (10)
F5—As1—F4	89.01 (13)	F11—As2—F6	83.45 (10)
F3—As1—F4	88.77 (12)	F7—As2—F6	84.98 (12)
F1—As1—F6	179.15 (10)	As2—F6—As1	148.45 (12)
F2—As1—F6	84.43 (11)	O1—C7—C1	179.0 (4)
F5—As1—F6	85.32 (11)	C6—C1—C7	118.6 (3)
F3—As1—F6	86.31 (11)	C6—C1—C2	122.9 (3)
F4—As1—F6	86.28 (10)	C7—C1—C2	118.6 (3)
F10—As2—F9	95.68 (17)	C5—C6—C1	118.1 (3)
F10—As2—F8	90.21 (16)	C3—C2—C1	117.4 (3)
F9—As2—F8	95.17 (13)	C6—C5—C4	119.4 (4)

F10—As2—F11	90.11 (14)	C3—C4—C5	121.8 (4)
F9—As2—F11	93.85 (12)	C2—C3—C4	120.5 (3)
C7—C1—C6—C5	−179.9 (3)	C1—C6—C5—C4	0.0 (6)
C2—C1—C6—C5	0.0 (6)	C6—C5—C4—C3	0.6 (7)
C6—C1—C2—C3	−0.5 (6)	C1—C2—C3—C4	1.1 (6)
C7—C1—C2—C3	179.3 (4)	C5—C4—C3—C2	−1.2 (7)

Benzoyl fluoride (xl013)

Crystal data

C_7H_5FO
M_r = 124.11
Monoclinic, $P2_1/n$
a = 12.592 (3) Å
b = 7.2274 (17) Å
c = 13.473 (3) Å
β = 104.77 (2)°
V = 1185.6 (5) Å^3
Z = 8
$F(000)$ = 512
D_x = 1.391 Mg m^{-3}
Mo $K\alpha$ radiation, λ = 0.71073 Å
Cell parameters from 1538 reflections
θ = 3.1–28.0°
μ = 0.11 mm^{-1}
T = 114 K
Plate, colorless
0.50 × 0.49 × 0.11 mm

Data collection

Rigaku Xcalibur Sapphire3 diffractometer
Radiation source: Enhance (Mo) X-ray Source
Graphite monochromator
Detector resolution: 15.9809 pixels mm^{-1}
ω scans
Absorption correction: multi-scan (CrysAlis PRO; Rigaku OD, 2020)
T_{min} = 0.151, T_{max} = 1.000
7905 measured reflections
2413 independent reflections
1506 reflections with $I > 2\sigma(I)$
R_{int} = 0.064
θ_{max} = 26.4°, θ_{min} = 2.6°
h = −12→15
k = −9→8
l = −16→16

Refinement

Refinement on F^2
Least-squares matrix: full
$R[F^2 > 2\sigma(F^2)]$ = 0.080
$wR(F^2)$ = 0.249
S = 1.04
2413 reflections
203 parameters
0 restraints
Primary atom site location: structure-invariant direct methods
Secondary atom site location: difference Fourier map
Hydrogen site location: difference Fourier map
All H-atom parameters refined
$w = 1/[\sigma^2(F_o^2) + (0.143P)^2]$ where $P = (F_o^2 + 2F_c^2)/3$
$(\Delta/\sigma)_{max} < 0.001$
$\Delta\rho_{max}$ = 0.38 e Å^{-3}
$\Delta\rho_{min}$ = −0.42 e Å^{-3}

Special details

Geometry. All esds (except the esd in the dihedral angle between two l.s. planes) are estimated using the full covariance matrix. The cell esds are taken into account individually in the estimation of esds in distances, angles and torsion angles; correlations between esds in cell parameters are only used when they are defined by crystal symmetry. An approximate (isotropic) treatment of cell esds is used for estimating esds involving l.s. planes.

Refinement. Refinement of F^2 against ALL reflections. The weighted R-factor wR and goodness of fit S are based on F^2, conventional R-factors R are based on F, with F set to zero for negative F^2. The threshold expression of $F^2 > 2\text{sigma}(F^2)$ is used only for calculating R-factors(gt) etc. and is not relevant to the choice of reflections for refinement. R-factors based on F^2 are statistically about twice as large as those based on F, and R- factors based on ALL data will be even larger.

Fractional atomic coordinates and isotropic or equivalent isotropic displacement parameters (Å²)

	x	*y*	*z*	U_{iso}*/U_{eq}	Occ. (<1)
F1	0.59238 (17)	0.5149 (4)	0.32406 (15)	0.0589 (7)	0.5
O1	0.45998 (18)	0.3237 (4)	0.32708 (18)	0.0715 (8)	0.5
O1A	0.59238 (17)	0.5149 (4)	0.32406 (15)	0.0589 (7)	0.5
F1A	0.45998 (18)	0.3237 (4)	0.32708 (18)	0.0715 (8)	0.5
C1	0.6054 (2)	0.3488 (4)	0.4782 (2)	0.0374 (7)	
C2	0.5550 (2)	0.2381 (5)	0.5361 (3)	0.0436 (8)	
C3	0.6090 (3)	0.1912 (5)	0.6362 (2)	0.0470 (8)	
C4	0.7134 (2)	0.2601 (5)	0.6782 (2)	0.0436 (8)	
C5	0.7641 (2)	0.3718 (5)	0.6216 (2)	0.0435 (8)	
C6	0.7103 (2)	0.4186 (4)	0.5209 (2)	0.0393 (7)	
C7	0.5473 (3)	0.3944 (5)	0.3717 (3)	0.0509 (9)	
F2	0.77738 (15)	0.3170 (4)	0.27303 (14)	0.0589 (7)	0.5
O2	0.87605 (16)	0.4706 (4)	0.18904 (16)	0.0628 (7)	0.5
O2A	0.77738 (15)	0.3170 (4)	0.27303 (14)	0.0589 (7)	0.5
F2A	0.87605 (16)	0.4706 (4)	0.18904 (16)	0.0628 (7)	0.5
C8	0.7013 (2)	0.3574 (4)	0.09457 (19)	0.0352 (7)	
C9	0.6067 (2)	0.2643 (5)	0.0990 (2)	0.0418 (7)	
C10	0.5244 (2)	0.2387 (4)	0.0095 (3)	0.0446 (8)	
C11	0.5367 (2)	0.3058 (4)	−0.0831 (2)	0.0437 (8)	
C12	0.6309 (2)	0.3986 (5)	−0.0875 (2)	0.0431 (8)	
C13	0.7129 (2)	0.4271 (4)	0.0017 (2)	0.0392 (7)	
C14	0.7909 (2)	0.3877 (5)	0.1874 (2)	0.0500 (9)	
H1	0.485 (2)	0.179 (4)	0.503 (2)	0.041 (8)*	
H2	0.572 (2)	0.108 (5)	0.675 (3)	0.052 (9)*	
H3	0.753 (2)	0.227 (5)	0.751 (3)	0.046 (8)*	
H4	0.840 (3)	0.423 (5)	0.649 (3)	0.053 (9)*	
H5	0.743 (2)	0.498 (4)	0.477 (2)	0.039 (8)*	
H6	0.593 (3)	0.205 (6)	0.163 (3)	0.077 (12)*	
H7	0.460 (3)	0.170 (5)	0.013 (2)	0.051 (9)*	
H9	0.636 (2)	0.473 (5)	−0.153 (2)	0.042 (8)*	
H10	0.786 (2)	0.500 (5)	0.000 (2)	0.045 (8)*	
H8	0.480 (3)	0.287 (6)	−0.145 (3)	0.084 (13)*	

Atomic displacement parameters (Å²)

	U^{11}	U^{22}	U^{33}	U^{12}	U^{13}	U^{23}
F1	0.0637 (13)	0.0711 (17)	0.0428 (11)	0.0145 (11)	0.0154 (9)	0.0138 (10)
O1	0.0633 (14)	0.076 (2)	0.0611 (15)	0.0057 (12)	−0.0093 (11)	−0.0072 (12)
O1A	0.0637 (13)	0.0711 (17)	0.0428 (11)	0.0145 (11)	0.0154 (9)	0.0138 (10)
F1A	0.0633 (14)	0.076 (2)	0.0611 (15)	0.0057 (12)	−0.0093 (11)	−0.0072 (12)
C1	0.0397 (15)	0.0327 (17)	0.0391 (16)	0.0066 (11)	0.0089 (11)	−0.0038 (12)
C2	0.0349 (15)	0.043 (2)	0.0524 (18)	0.0034 (12)	0.0102 (13)	−0.0049 (14)
C3	0.0498 (17)	0.048 (2)	0.0474 (18)	0.0084 (14)	0.0195 (14)	0.0106 (15)
C4	0.0424 (16)	0.053 (2)	0.0354 (16)	0.0091 (13)	0.0105 (12)	0.0014 (14)
C5	0.0419 (16)	0.044 (2)	0.0438 (17)	0.0036 (13)	0.0097 (12)	−0.0086 (14)

C6	0.0455 (16)	0.0326 (18)	0.0427 (16)	0.0012 (12)	0.0165 (12)	0.0011 (13)
C7	0.0528 (18)	0.049 (2)	0.0460 (17)	0.0153 (15)	0.0045 (14)	−0.0066 (16)
F2	0.0492 (12)	0.090 (2)	0.0351 (11)	0.0119 (10)	0.0069 (8)	0.0054 (10)
O2	0.0478 (12)	0.0733 (18)	0.0615 (14)	0.0005 (10)	0.0031 (9)	−0.0111 (11)
O2A	0.0492 (12)	0.090 (2)	0.0351 (11)	0.0119 (10)	0.0069 (8)	0.0054 (10)
F2A	0.0478 (12)	0.0733 (18)	0.0615 (14)	0.0005 (10)	0.0031 (9)	−0.0111 (11)
C8	0.0363 (14)	0.0333 (17)	0.0350 (15)	0.0078 (11)	0.0073 (11)	−0.0019 (12)
C9	0.0454 (16)	0.0397 (19)	0.0435 (17)	0.0056 (12)	0.0173 (13)	0.0055 (13)
C10	0.0375 (16)	0.041 (2)	0.0544 (19)	−0.0054 (13)	0.0110 (13)	−0.0040 (14)
C11	0.0409 (16)	0.0418 (19)	0.0428 (17)	0.0007 (13)	0.0007 (12)	−0.0065 (14)
C12	0.0479 (17)	0.042 (2)	0.0403 (16)	−0.0012 (13)	0.0122 (12)	0.0012 (13)
C13	0.0401 (15)	0.0327 (18)	0.0451 (16)	−0.0042 (12)	0.0115 (11)	−0.0028 (13)
C14	0.0459 (18)	0.054 (2)	0.0437 (18)	0.0160 (15)	0.0000 (13)	−0.0073 (15)

Geometric parameters (Å, º)

F1—C7	1.295 (4)	F2—C14	1.312 (4)
O1—C7	1.223 (4)	O2—C14	1.223 (4)
O1A—C7	1.295 (4)	O2A—C14	1.312 (4)
F1A—C7	1.223 (4)	F2A—C14	1.223 (4)
C1—C2	1.380 (4)	C8—C9	1.382 (4)
C1—C6	1.394 (4)	C8—C13	1.391 (4)
C1—C7	1.472 (4)	C8—C14	1.472 (4)
C2—C3	1.389 (5)	C9—C10	1.388 (4)
C3—C4	1.385 (5)	C10—C11	1.384 (5)
C4—C5	1.375 (5)	C11—C12	1.377 (4)
C5—C6	1.394 (4)	C12—C13	1.385 (4)
C2—C1—C6	120.0 (3)	C9—C8—C13	120.3 (3)
C2—C1—C7	119.7 (3)	C9—C8—C14	121.2 (3)
C6—C1—C7	120.3 (3)	C13—C8—C14	118.4 (3)
C1—C2—C3	120.5 (3)	C8—C9—C10	119.2 (3)
C4—C3—C2	119.2 (3)	C11—C10—C9	120.4 (3)
C5—C4—C3	120.8 (3)	C12—C11—C10	120.3 (3)
C4—C5—C6	120.2 (3)	C11—C12—C13	119.6 (3)
C1—C6—C5	119.3 (3)	C12—C13—C8	120.0 (3)
O1—C7—F1	119.4 (3)	O2—C14—F2	119.0 (3)
F1A—C7—O1A	119.4 (3)	F2A—C14—O2A	119.0 (3)
F1A—C7—C1	123.1 (3)	F2A—C14—C8	124.6 (3)
O1—C7—C1	123.1 (3)	O2—C14—C8	124.6 (3)
F1—C7—C1	117.5 (3)	F2—C14—C8	116.5 (3)
O1A—C7—C1	117.5 (3)	O2A—C14—C8	116.5 (3)
C6—C1—C2—C3	−1.7 (5)	C13—C8—C9—C10	1.0 (5)
C7—C1—C2—C3	179.0 (3)	C14—C8—C9—C10	−179.9 (3)
C1—C2—C3—C4	1.4 (5)	C8—C9—C10—C11	−0.1 (5)
C2—C3—C4—C5	−0.8 (5)	C9—C10—C11—C12	0.1 (5)
C3—C4—C5—C6	0.6 (5)	C10—C11—C12—C13	−1.0 (5)

C2—C1—C6—C5	1.4 (4)	C11—C12—C13—C8	1.9 (5)
C7—C1—C6—C5	−179.3 (3)	C9—C8—C13—C12	−1.9 (4)
C4—C5—C6—C1	−0.8 (5)	C14—C8—C13—C12	179.0 (3)
C2—C1—C7—F1A	−7.8 (5)	C9—C8—C14—F2A	−179.1 (3)
C6—C1—C7—F1A	172.9 (3)	C13—C8—C14—F2A	−0.1 (5)
C2—C1—C7—O1	−7.8 (5)	C9—C8—C14—O2	−179.1 (3)
C6—C1—C7—O1	172.9 (3)	C13—C8—C14—O2	−0.1 (5)
C2—C1—C7—F1	172.4 (3)	C9—C8—C14—F2	2.0 (4)
C6—C1—C7—F1	−6.9 (4)	C13—C8—C14—F2	−178.9 (3)
C2—C1—C7—O1A	172.4 (3)	C9—C8—C14—O2A	2.0 (4)
C6—C1—C7—O1A	−6.9 (4)	C13—C8—C14—O2A	−178.9 (3)